Article published online: 2022-03-24

Original Article

(18F)-Fluorodeoxyglucose positron emission tomography/magnetic resonance imaging assessment of hypometabolism patterns in clinical phenotypes of suspected corticobasal degeneration

ABSTRACT

Corticobasal degeneration (CBD) is a rare neurodegenerative disorder presenting with atypical parkinsonian symptoms that characteristically involves the frontoparietal region including the primary sensorimotor cortex, ipsilateral basal ganglia, and thalamus, typically in an asymmetric pattern. We aim to evaluate the metabolic and volumetric abnormalities in patients with clinically suspected CBD phenotypes utilizing hybrid ^{18}F-fluorodeoxyglucose (FDG) positron emission tomography–magnetic resonance (PET/MR) brain imaging. A retrospective analysis was performed on 75 patients (mean age 74 years, 31 males and 44 females) who underwent ^{18}F-FDG PET/MR imaging (MRI) as part of their clinical dementia workup. Images were obtained using an integrated Siemens mMR 3T PET/MRI scanner. Two board-certified neuroradiologists and a nuclear medicine physician evaluated the metabolic and volumetric data of each hemisphere to assess for symmetric or asymmetric involvement of regions of interest in the subset of patients with suspected CBD. Of the 75 patients, 12 were diagnosed with suspected CBD based on a combination of clinical symptoms, neurocognitive testing, and hybrid neuroimaging findings. Ten of 12 patients (87%) demonstrated asymmetrically decreased FDG uptake involving a single cerebral hemisphere and ipsilateral subcortical structures, whereas two of 12 patients (13%) demonstrated striking hypometabolism of the bilateral sensorimotor cortices. Our study highlights two characteristic patterns of hypometabolism in patients with clinical and neuroimaging findings suggestive of the underlying CBD. The first pattern is asymmetric hypometabolism and volume loss, particularly within the frontoparietal and occipital cortices with involvement of ipsilateral subcortical structures, including the basal ganglia and thalamus. The second, more atypical pattern, is symmetric hypometabolism with striking involvement of the bilateral sensorimotor cortices.

Keywords: Corticobasal degeneration, fluorodeoxyglucose, hybrid neuroimaging, positron emission tomography/magnetic resonance imaging

Ana M. Franceschi, Michael Clifton[1], Kiyon Naser-Tavakolian[1], Osama Ahmed[1], Giuseppe Cruciata[1], Lev Bangiyev[1], Sean Clouston[2], Dinko Franceschi[1]

Department of Radiology, Neuroradiology Section, Donald and Barbara Zucker School of Medicine at Hofstra/Northwell Health, Manhasset, Departments of [1]Radiology and [2]Family, Population and Preventative Medicine, SUNY Stony Brook, Stony Brook, NY, USA

Address for correspondence: Dr. Osama Ahmed, Department of Radiology, 101 Nicolas Road, Stony Brook, NY 11794, USA.
E-mail: osama.ahmed@stonybrookmedicine.edu

Submitted: 24-Apr-2020, **Revised:** 22-May-2020, **Accepted:** 06-Jun-2020, **Published:** 07-Oct-2020

INTRODUCTION

According to the Census Bureau, the United States of America is projected to retain its position as the second oldest country in the world in 2050, with 21.4% of the population aged 65 years or older. Moreover, this number is projected to increase from 73.5 million to 98.2 million by 2060.[1] Furthermore, clinically significant cognitive impairment affects more than 14% of the population over 65 years of age and more than 50% of

Access this article online	
Website: www.wjnm.org	Quick Response Code
DOI: 10.4103/wjnm.WJNM_62_20	

How to cite this article: Franceschi AM, Clifton M, Naser-Tavakolian K, Ahmed O, Cruciata G, Bangiyev L, *et al.* (18F)-Fluorodeoxyglucose positron emission tomography/magnetic resonance imaging assessment of hypometabolism patterns in clinical phenotypes of suspected corticobasal degeneration. World J Nucl Med 2021;20:176-84.

individuals older than 85 years.[2] If this pattern continues, we can conservatively estimate approximately 13.8 million Americans to have a diagnosis of dementia by 2060.

Neurodegenerative disorders are the leading cause of geriatric cognitive impairment and are characterized by progressive, cumulative damage to neuronal structure and interconnectivity, with a range of clinical symptoms including memory loss, decline in executive function, and behavioral changes leading to social and occupational dysfunction. Correctly diagnosing the etiology of cognitive impairment is becoming increasingly important for treatment and clinical management strategies.[3,4] However, accurate diagnosis is challenging for many clinicians, especially in the early stages of disease presentation. The utilization of advanced neuroimaging techniques which combine anatomical information with functionality is playing an increasingly important role in the diagnosis of many dementia subtypes. Specifically, combining functional, metabolic, and neurotransmitter release data from brain positron emission tomography (PET) imaging with anatomic information from structural magnetic resonance imaging (MRI) sequences allows for precise and accurate characterization of brain regions that may be dysfunctional, thus suggesting the underlying neurodegenerative disorder, even before overt clinical symptomatology.[4-7] These data can empower the clinician with improved diagnostic capability, management of disease progression, and evaluation of possible responses to novel dementia therapeutics.

Among the causes of dementia, corticobasal degeneration (CBD) is a rare diagnosis which is accurately predicted in significantly less than half of pathologically confirmed cases antemortem.[6] Clinically, patients with suspected CBD demonstrate a progressive movement and neurodegenerative disorder with asymmetric symptoms, primarily characterized by apraxia, dystonia, postural instability, and an akinetic-rigid syndrome that does not respond to levodopa.[3] Notably, it is a neurodegenerative disorder that is associated with abnormal tau protein aggregates which form neurofibrillary tangles, the primary histopathologic feature of CBD. Collectively, the term "tauopathies" encompasses multiple neurodegenerative processes, including Alzheimer's dementia, frontotemporal dementia subtypes, including the atypical parkinsonian syndromes such as CBD and progressive supranuclear palsy (PSP). There exists an overlap of clinical phenotypes within the tauopathies, which makes distinguishing these entities difficult, especially in daily clinical practice. Particularly, CBD and PSP are genetically related, but clinically distinct causes of progressive motor dysfunction and cognitive impairment. Both diseases present with atypical parkinsonism (dystonia, cognitive impairment, and eye movement disorders) and a documented history of resistance to levodopa treatment.[5] For example, in a recent case series by Litvan *et al*., of 34 patients that were initially diagnosed with CBD, 16 were found to have neuropathologic confirmation of PSP at postmortem analysis.[6]

There is limited information in the literature regarding the metabolic and volumetric changes in patients presenting clinically with atypical parkinsonism, in particular, those with clinical symptoms compatible with the underlying CBD. Notably, prior studies have primarily focused on anatomic information and structural MRI data to assess for pertinent morphological changes, which are most commonly found in the pre/postcentral gyri, basal ganglia, and posterolateral putamen.[8-10] These changes are, unfortunately, nonspecific and seen in a multitude of pathologies affecting the brain.

In this study, we present a series of patients presenting to dementia/movement disorder clinics at our institution with atypical parkinsonism and clinically suspected CBD, who then underwent hybrid ^{18}F-fluorodeoxyglucose (FDG) PET/magnetic resonance (MR) brain imaging, including metabolic and volumetric analysis, as part of their routine clinical dementia workup.

MATERIALS AND METHODS

Ethics

This study received local institutional review board (IRB) approval. The IRB waived the need for written informed consent given the retrospective nature of the study.

The patients presented to the neurological clinics with cognitive impairment and atypical parkinsonian features, for which they underwent brain ^{18}F-FDG PET/MRI as part of their clinical dementia workup. Our exclusion criteria included patients younger than 18 years old, those with a clinical indication other than dementia, pregnant women, and patients with a fasting blood glucose level >150 mg/dL. Additional technical exclusions included patients with PET/MRI scans without dedicated brain sequences, deviation from standard protocol sequence acquisition, or non-FDG PET/MRI studies.

Prior to imaging, an injection of 5 mCi of FDG was administered intravenously. After 40 min of uptake, the patients were positioned for brain imaging in a Siemens mMR 3T PET/MRI (Siemens Healthcare, Erlangen, Germany) scanner with a standard 12-channel head coil. A dual-echo T1-weighted gradient-recalled echo sequence was performed

to acquire the MRI attenuation-correction map based on a Dixon segmentation (air, fat, soft tissue, and lungs). Emission data were collected for 20 min during the time in which the dedicated brain MR sequences were acquired. PET data were reconstructed with an iterative 3D ordinary Poisson-ordered subset expectation-maximization algorithm at 3 iterations and 21 subsets and with a 4-mm Gaussian postreconstruction image filter. PET image matrix size was 344 mm × 344 mm × 127 mm, and trans-axial voxel dimensions were 1.04 mm × 1.04 mm with a thickness of 2.03 mm.

The postprocessing of PET images was performed utilizing a custom-built workflow with MIMneuro version 6.9.5 (MIM Software, Inc., Cleveland, OH, USA), including semi-quantitative analyses of age-matched Z-score FDG brain data.

MRI data included images from the skull vertex to the foramen magnum. Standard high-resolution 3D Sagittal MPRAGE and 3D fluid-attenuated inversion recovery (FLAIR) sequences were used for brain anatomy. Afterward, routine diagnostic MRI sequences including T2 Turbo Spin Echo (TSE) in the axial and coronal planes, axial susceptibilityweighted imaging (SWI), diffusion tensor imaging (DTI), proton density (PD) axial imaging, and diffusionweighted imaging was obtained.

3D MPRAGE image data were additionally postprocessed by NeuroQuant (2019 CorTechs Labs, Inc San Diego, CA, USA) for semi-quantitative volumetric analysis.

The 3D FLAIR fat-suppressed sagittal images were obtained using the following parameters: repetition time/echo time/inversion time (TI) of 5000 ms/402 ms/1800 ms, respectively; a field of view (FOV) of 250 mm; voxel size of 0.9 mm × 0.9 mm × 0.9 mm; slice thickness 0.9 mm; and an acquisition time of 7 min. The 3D sagittal MPRAGE sequence was obtained using a repetition time/echo time/TI of 1700 ms/2.44 ms/841 ms, respectively; FOV of 250 mm; voxel size of 1.0 mm × 1.0 mm × 1.0 mm; slice thickness 1.0 mm; flip angle of 9°; and acquisition time of 3 min and 58 s. MR-based attenuation-corrected PET sequence was obtained using a repetition time/echo time 1 and echo time 2 of 3.6 ms/1.23 ms and 2.46 ms, respectively; FOV of 500 mm; voxel size of 4.2 mm × 2.6 mm × 3.1 mm; slice thickness of 3.12 mm; flip angle of 10°; and acquisition time of 19 s. DTI sequence was obtained using the following parameters: repetition time/echo time 5600 ms/90 ms; FOV of 250 mm; voxel size of 2.0 mm × 2.0 mm × 4.0 mm; slice thickness of 4 mm; delay of 0 ms; and an acquisition time of 3 min and 10 s. T2 TSE in the axial plane was obtained using the following parameters: repetition time/echo time of 4000 ms/96.0 ms; FOV of 230 mm; voxel size of 0.8 mm × 0.7 mm × 3.0 mm; slice thickness of 3.0 mm with 0 ms of delay; flip angle of 150°; and acquisition time of 1 min and 12 s. T2 TSE in the coronal plane was obtained using the following parameters: repetition time/echo time of 4720 ms/96.0 ms, FOV of 230 mm; voxel size of 0.8 mm × 0.7 mm × 3.0 mm; slice thickness of 3.0 mm with 0 ms of delay; flip angle of 150°; and acquisition time of 1 min and 25 s. SWI was obtained in the axial plane using the following parameters: repetition time/echo time of 26 ms/20 ms, FOV of 230 mm; voxel size of 0.8 mm × 0.7 mm × 1.3 mm; slice thickness of 1.3 mm; flip angle of 15°; and acquisition time of 5 min and 2 s. Diffusion images were obtained using the following parameters: repetition time/echo time of 7500 ms/92.0 ms, FOV of 240 mm; voxel size of 1.5 mm × 1.5 mm × 4.0 mm; slice thickness of 4.0 mm with 0 ms of delay; and acquisition time of 2 min and 8 s. PD axial images were obtained using the following parameters: repetition time/echo time 1 and 2 of 2800 ms/10 ms and 93 ms; FOV of 230 mm; voxel size of 0.9 mm × 0.9 mm × 3.0 mm; slice thickness of 3.0 mm with 0 ms of delay; flip angle of 150°; and acquisition time of 2 min and 41 s.

Patient selection and image analysis

The patients were referred from dementia/movement disorder clinics for ^{18}F-FDG PET/MRI as part of their clinical evaluation for signs and symptoms of dementia. A total of 75 patients with neuropsychological and cognitive testing suggestive of underlying neurodegenerative disorder were included in this study. The imaging findings in the subset of patients with suspected CBD were then discussed with the referring clinician by our neuroradiologists and nuclear medicine physician prior to consensus.

Two neuroradiology fellowship-trained board-certified radiologists with dedicated PET/MRI clinical and research expertise interpreted the fused brain PET/MRI sequences including Neuroquant semi-quantitative volumetric data and classified each dementia subtype blinded to clinical history and neurologic exam findings. Along with qualitative assessment, 3D MPRAGE MR image data were additionally evaluated by NeuroQuant (2019 CorTechs Labs, Inc. San Diego, California, USA) for quantitative volumetric analysis. NeuroQuant is a Food and Drug Administration-cleared software that analyzes intracranial volume and compares these volumes to a normative database. NeuroQuant compares lobar and sub-lobar cortical volumes to their standardized database, which are adjusted for age, sex, and volume status. Regions of parenchymal volume loss >2 standard deviations from normal controls in the standardized atlas were flagged as abnormal. Quantitative percentages were assigned to lobar and sub-lobar areas to quantify the extent of parenchymal volume loss. Of note, NeuroQuant software provides semi-quantitative data

regarding the aforementioned variables and does not provide a dementia diagnosis.

One nuclear medicine physician with 25 years of experience in brain PET imaging then separately interpreted the PET portion of each PET/MRI brain study with additional surface map reconstructions, fused transaxial images, and analysis of Z-score metabolic data utilizing MIMneuro version 6.9.5. MIMneuro software runs a region-based analysis which calculates Z-scores (number of standard deviations from the mean) and asymmetry measurements for individual brain regions defined by the Single Brain Atlas and MIM Probabilistic anatomical atlas to provide semi-quantitative analysis of hypometabolism. According to the manufacturer, the Single Brain Atlas and MIM Probabilistic anatomical atlas is composed of 43 individuals (19 females and 24 males) with an age range of 41–80 years. The distribution of the normal age-based atlas is as follows: six patients aged 40–49, eight patients aged 50–59, 14 patients aged 60–69, 14 patients aged 70–79, and one patient aged between 80 and 89. The mean age and standard deviation of these 43 individuals are 63.8 ± 9.98 years. The automated Z-scores are calculated by comparing the patient to the selected age-matched set of normal controls (within 5 years of the patient's age). Of note, MIMneuro software provides semi-quantitative score analysis regarding the aforementioned variables and does not provide a dementia diagnosis.

The subset of patients demonstrating imaging findings suggestive of CBD were marked independently on data collection sheets. After analysis of all the study patients, a group review of positive cases was then conducted, whereby any discrepancy was resolved by a consensus review among the three readers. Supratentorial parenchymal FDG uptake was scored by each reader as follows: symmetrical, asymmetrical L > R, and asymmetrical R > L cortical atrophy and radiotracer uptake. Following supratentorial analysis, subcortical structures, specifically basal ganglia and thalami, were assessed for volumetric and metabolic changes. Subcortical FDG uptake was scored as follows: symmetrical or asymmetrical radiotracer uptake.

FDG activity normalization was scaled to the whole cerebellum, unless patients were found to have asymmetric cerebellar FDG uptake, in which case the supratentorial brain uptake was scaled to pontine uptake values. Recent reports in the literature with various brain PET tracers investigating neurodegenerative diseases have demonstrated variabilities associated with cerebellar normalization of PET images. Moreover, the utilization of the pons as a reference region has reduced variabilities in the longitudinal progression of disease entities that involve amyloid deposition and, to a lesser extent, tau.[11-14]

Statistical analysis

Descriptive characteristics were provided using averages, standard deviation, and percentiles. The types and numbers of final diagnoses were also determined. Semi-quantitative data were compared across hemispheres using two-tailed Student's *t*-test. Values of $P < 0.05$ were considered statistically significant.

RESULTS

Twelve cases in our dataset of 75 patients demonstrated imaging and clinical findings compatible with eventual diagnosis of CBD.

The available clinical data including age, sex, Montreal Cognitive Assessment (MoCA) scores, and symptomatology for the 12 cases with suspected CBD are summarized in Table 1. Common presenting symptoms were elicited at our institutional dementia/movement disorder clinics by a multidisciplinary team including a board-certified neurologist specializing in neurodegeneration and a behavioral psychologist. The average and range of MoCA scores are displayed in the third column (score of 26/30 or higher is normal). Documented clinical symptoms were present for a minimum of 1 year and are listed in descending order by prevalence. The far-right column presents relevant findings within individual neurocognitive exams, in descending order.

Table 1: Clinical and demographic data of patients with suspected CBD on the basis of clinical assessment and imaging findingsl

Number of Patients by Sex	Average Age	Average MoCA score (range)	*Common Presenting Symptoms that are present for > 1 year*	*Common Findings on Neurocognitive Testing*
3 Male 9 Female	74.6	21.2 (15-23) Standard Devation 3.3	Progressive memory loss (10/12) Gait Disturbance (5/12) Behavioral changes (3/12)	Delayed recall (7/12) Impaired clock drawing (7/12) Visio-spatial memory (7/12) Gait ataxia (5/12) Language deficit (3/12) Visio-spatial deficits (3/12) Dysdiadochokinesia (2/12)

On (F18)-FDG PET/MR brain imaging, 10 of the 12 patients with suspected CBD demonstrated characteristic asymmetrically decreased supratentorial FDG uptake, with hypometabolism involving a single hemisphere and subcortical structures, including the ipsilateral basal ganglia and thalamus. These same patients had clinical symptoms more pronounced on the contralateral side. Two of the twelve patients had a more atypical, symmetric pattern of decreased supratentorial FDG uptake, with striking involvement of the bilateral sensorimotor cortices. These patients demonstrated relatively symmetric clinical symptoms. The regions of interest (ROIs) that best separated our CBD cases from other neurodegenerative diseases included the frontoparietal sensorimotor cortex (precentral and postcentral gyri), occipital lobe, thalamus, and basal ganglia.

Within the ten patients with a markedly asymmetric pattern of hypometabolism between the left and right cerebral hemispheres, the findings were particularly pronounced in the sensorimotor cortex of the frontoparietal lobes, precuneus, and occipital lobe of the affected cerebral hemisphere. Additional ROIs within the ipsilateral subcortical structures, including the basal ganglia and thalamus, also demonstrated markedly asymmetric FDG uptake. In these patients with striking hemispheric asymmetry, the primary motor cortex (precentral gyrus) average metabolic FDG Z-scores generated by MIMneuro software in the affected and unaffected sides were −3.6 versus −1.46, respectively ($P = 0.011$). The primary sensory cortex (postcentral gyrus) had average Z-scores of −2.93 versus −0.62 in the affected and unaffected sides, respectively ($P = 0.05$). Furthermore, the majority of patients with asymmetric patterns (72%) also demonstrated corresponding atrophy on structural MRI with ipsilateral sensorimotor cortex volumes in the $<5^{th}$ percentile for age per semi-quantitative Neuroquant analysis. In most cases, as detailed by the symptomatology in Table 1, these imaging findings corresponded with the patient's side of symptoms.

Figures 1a-e demonstrates an example of a patient with clinical and imaging findings most suggestive of CBD, with striking hemispheric asymmetry in radiotracer uptake. Cortical surface maps [Figure 1a] demonstrate markedly reduced FDG uptake within nearly the entire left cerebral hemisphere, including markedly decreased radiotracer uptake in the left sensorimotor cortex, left basal ganglia, left thalamus, left anterior and mid cingulate gyrus, and in the left occipital lobe. These findings are further highlighted on the trans-axial fusion FLAIR and FDG-PET views [Figure 1b], a select fusion FLAIR/PET axial image through the subcortical structures [Figure 1c] and on the FLAIR MRI and FDG-PET images with semi-quantitative Z-score overlays [Figure 1d], which provide more insight into the anatomy and distribution of left-dominant hypometabolism patterns. Semi-quantitative analysis of FDG brain Z-scores calculated in comparison to age-matched normal controls in tabular format [Figure 1e] for this patient also revealed markedly decreased values in numerous regions of the left cerebral hemisphere, including statistically significant decreased FDG uptake values for age in the precentral and postcentral gyri of the left sensorimotor cortex (Z-scores of −2.8 and −2.3, respectively).

Two of the twelve patients with suspected CBD demonstrated a more atypical pattern of symmetrically decreased FDG uptake, which was most striking in the bilateral pre- and postcentral gyri of the primary sensorimotor cortex, with corresponding volumetric abnormalities in these ROIs on anatomic MRI sequences. For example, in the first case, hypometabolism in the primary motor cortex (precentral gyrus) demonstrated statistically significant decreased FDG Z-score values of −1.88 on the left and −1.69 on the right and within the primary sensory cortex (postcentral gyrus), a Z-score of −1.66 on the left and −1.95 on the right.

Figure 2a-e provides an example of a patient with clinical and imaging findings most suggestive of CBD with symmetric imaging pattern, including striking hypometabolism in the bilateral sensorimotor cortices. Cortical surface maps [Figure 2a] demonstrate abnormal FDG distribution patterns with moderately decreased tracer activity within the bilateral frontoparietal region, specifically involving the postcentral and precentral gyri bilaterally with preserved normal radiotracer uptake in the subcortical structures including in the thalami and basal ganglia. These findings are further highlighted on the transaxial fusion FLAIR and FDG-PET views [Figure 2b], select fusion FLAIR/PET axial image through the sensorimotor cortex and coronal image through the subcortical structures [Figure 2c], and FLAIR MRI and FDG-PET images with semi-quantitative Z-score overlays [Figure 2d], which also allows for more detailed anatomic localization. Semi-quantitative analysis using Z-scores calculated in comparison to age-matched healthy controls [Figure 2e] confirmed significantly decreased values in the bilateral parietal lobes, including in precentral and postcentral gyri of the sensorimotor cortex (Z-scores of −1.88 and −1.66 in the left and −1.69 and −1.95 in the right precentral and postcentral gyri, respectively). While these findings could relate to a similar clinical entity such as PSP, the predominant pathological imaging features were more pronounced in the pre/post central gyri, thalami, and subcortical structures, which allowed us to suggest pathology more consistent with CBD rather than PSP, which typically

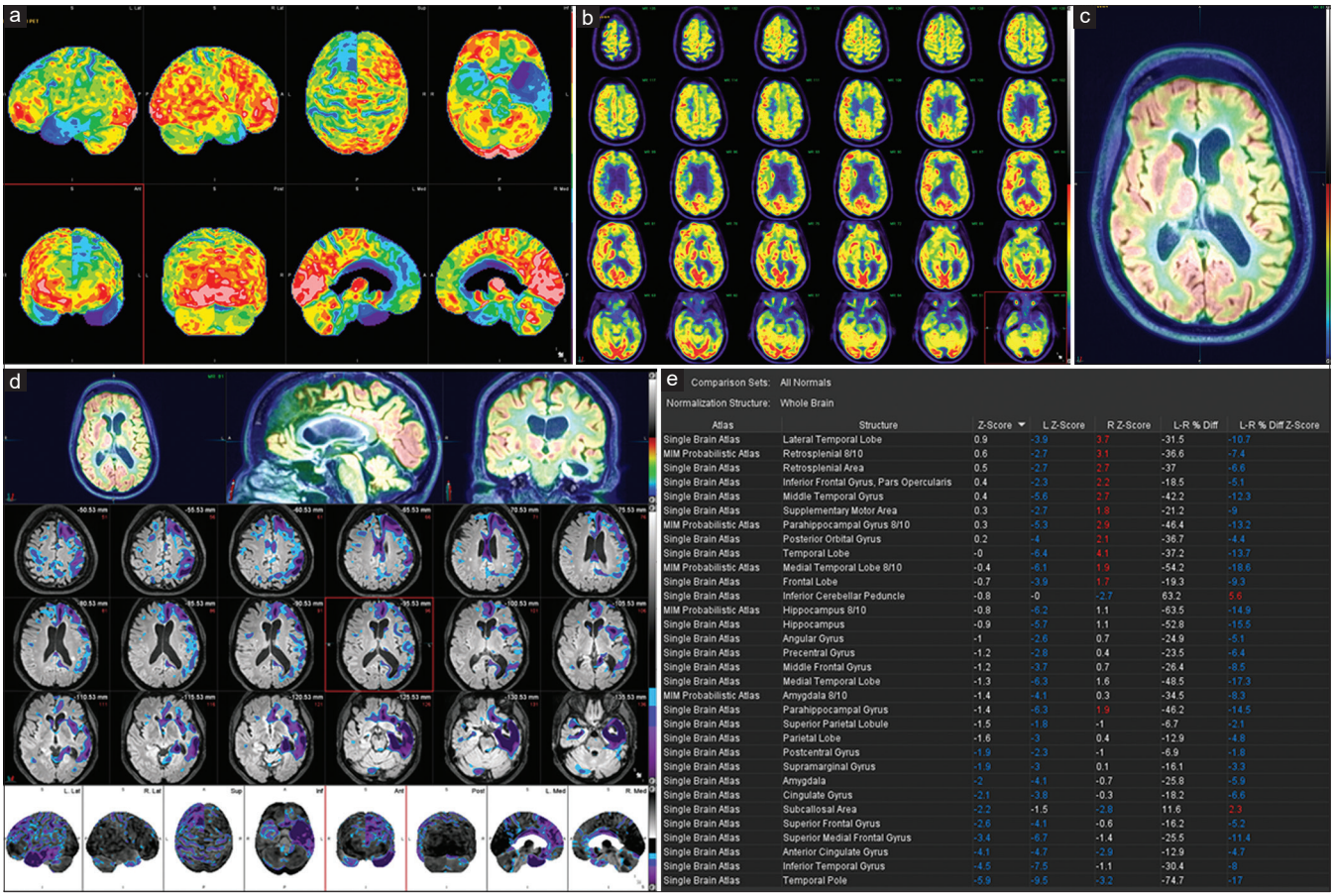

Atlas	Structure	Z-Score	L Z-Score	R Z-Score	L-R % Diff	L-R % Diff Z-Score
Single Brain Atlas	Lateral Temporal Lobe	0.9	-3.9	3.7	-31.5	-10.7
MIM Probabilistic Atlas	Retrosplenial 8/10	0.6	-2.7	3.1	-36.6	-7.4
Single Brain Atlas	Retrosplenial Area	0.5	-2.7	2.7	-37	-6.6
Single Brain Atlas	Inferior Frontal Gyrus, Pars Opercularis	0.4	-2.3	2.2	-18.5	-5.1
Single Brain Atlas	Middle Temporal Gyrus	0.4	-5.6	2.7	-42.2	-12.3
Single Brain Atlas	Supplementary Motor Area	0.3	-2.7	1.8	-21.2	-9
MIM Probabilistic Atlas	Parahippocampal Gyrus 8/10	0.3	-5.3	2.9	-46.4	-13.2
Single Brain Atlas	Posterior Orbital Gyrus	0.2	-4	2.1	-36.7	-4.4
Single Brain Atlas	Temporal Lobe	-0	-6.4	4.1	-37.2	-13.7
MIM Probabilistic Atlas	Medial Temporal Lobe 8/10	-0.4	-6.1	1.9	-54.2	-18.6
Single Brain Atlas	Frontal Lobe	-0.7	-3.9	1.7	-19.3	-9.3
Single Brain Atlas	Inferior Cerebellar Peduncle	-0.8	-0	-2.7	63.2	5.6
MIM Probabilistic Atlas	Hippocampus 8/10	-0.8	-6.2	1.1	-63.5	-14.9
Single Brain Atlas	Hippocampus	-0.9	-5.7	1.1	-52.8	-15.5
Single Brain Atlas	Angular Gyrus	-1	-2.6	0.7	-24.9	-5.1
Single Brain Atlas	Precentral Gyrus	-1.2	-2.8	0.4	-23.5	-6.4
Single Brain Atlas	Middle Frontal Gyrus	-1.2	-3.7	0.7	-26.4	-8.5
Single Brain Atlas	Medial Temporal Lobe	-1.3	-6.3	1.6	-48.5	-17.3
MIM Probabilistic Atlas	Amygdala 8/10	-1.4	-4.1	0.3	-34.5	-8.3
Single Brain Atlas	Parahippocampal Gyrus	-1.4	-6.3	1.9	-46.2	-14.5
Single Brain Atlas	Superior Parietal Lobule	-1.5	-1.8	-1	-6.7	-2.1
Single Brain Atlas	Parietal Lobe	-1.6	-3	0.4	-12.9	-4.8
Single Brain Atlas	Postcentral Gyrus	-1.9	-2.3	-1	-6.9	-1.8
Single Brain Atlas	Supramarginal Gyrus	-1.9	-3	0.1	-16.1	-3.3
Single Brain Atlas	Amygdala	-2	-4.1	-0.7	-25.8	-5.9
Single Brain Atlas	Cingulate Gyrus	-2.1	-3.8	-0.3	-18.2	-6.6
Single Brain Atlas	Subcallosal Area	-2.2	-1.5	-2.8	11.6	2.3
Single Brain Atlas	Superior Frontal Gyrus	-2.6	-4.1	-0.6	-16.2	-5.2
Single Brain Atlas	Superior Medial Frontal Gyrus	-3.4	-6.7	-1.4	-25.5	-11.4
Single Brain Atlas	Anterior Cingulate Gyrus	-4.1	-4.7	-2.9	-12.9	-4.7
Single Brain Atlas	Inferior Temporal Gyrus	-4.5	-7.5	-1.1	-30.4	-8
Single Brain Atlas	Temporal Pole	-5.9	-9.5	-3.2	-74.7	-17

Figure 1: (a) Cortical fluorodeoxyglucose-positron emission tomography surface maps. (b) Transaxial fusion images (axial fluid-attenuated inversion recovery and positron emission tomography). (c) Select fusion fluid-attenuated inversion recovery/positron emission tomography axial image through the subcortical structures. (d) Fluid-attenuated inversion recovery-magnetic resonance imaging and positron emission tomography images with semi-quantitative Z-score overlays. (e) MIMneuro Z-score fluorodeoxyglucose brain data in tabular format

demonstrates volume loss in the midbrain and infratentorial ROIs. Moreover, correlation with the electronic medical record and neurology teams allowed us to confirm physical exam findings and neurocognitive testing data consistent with a predominant sensory/motor deficit with preserved language, which enhanced our diagnostic efficiency.

Notably, nine of the twelve patients demonstrated congruence of findings of metabolic and anatomic abnormalities where regions of hypometabolism corresponded to regions of volume loss, suggesting hypofunction of residual neurons in the regions affected by neurodegenerative process. The remaining three patients demonstrated hypometabolism without preferential volume loss on the affected side.

DISCUSSION

There is limited data in the scientific literature describing metabolic and volumetric changes in patients with atypical parkinsonian syndromes and in particular, those with suspected underlying CBD. Of note, prior imaging studies mainly describe structural changes that may support a clinical diagnosis of CBD; however, to date, the ability to accurately diagnose patients with CBD premortem is limited.[10]

Furthermore, it is essential to accurately distinguish between clinical symptomatology and histopathologic tissue classification of disease. CBD and corticobasal syndrome (CBS) are overlapping yet frequently confused terms used to define diseased tissue of neurons/glial cells, and the aforementioned symptomatology that precedes an eventual final tissue diagnosis.[6-8] Recent guidelines suggest that merely a diagnosis of CBD is no longer reflective of the clinicopathologic findings and that CBD exists as an umbrella term, encompassing four distinct clinical phenotypes: CBS, frontal behavioral-spatial syndrome, nonfluent/agrammatic variant of primary progressive aphasia, and PSP syndrome (PSPS).[9] Therefore, while PSPS may present clinically as CBD phenotype, it is much more likely to represent PSP on histopathology, rather than underlying CBD *per se*. This specific dilemma demands careful imaging correlation with neurocognitive

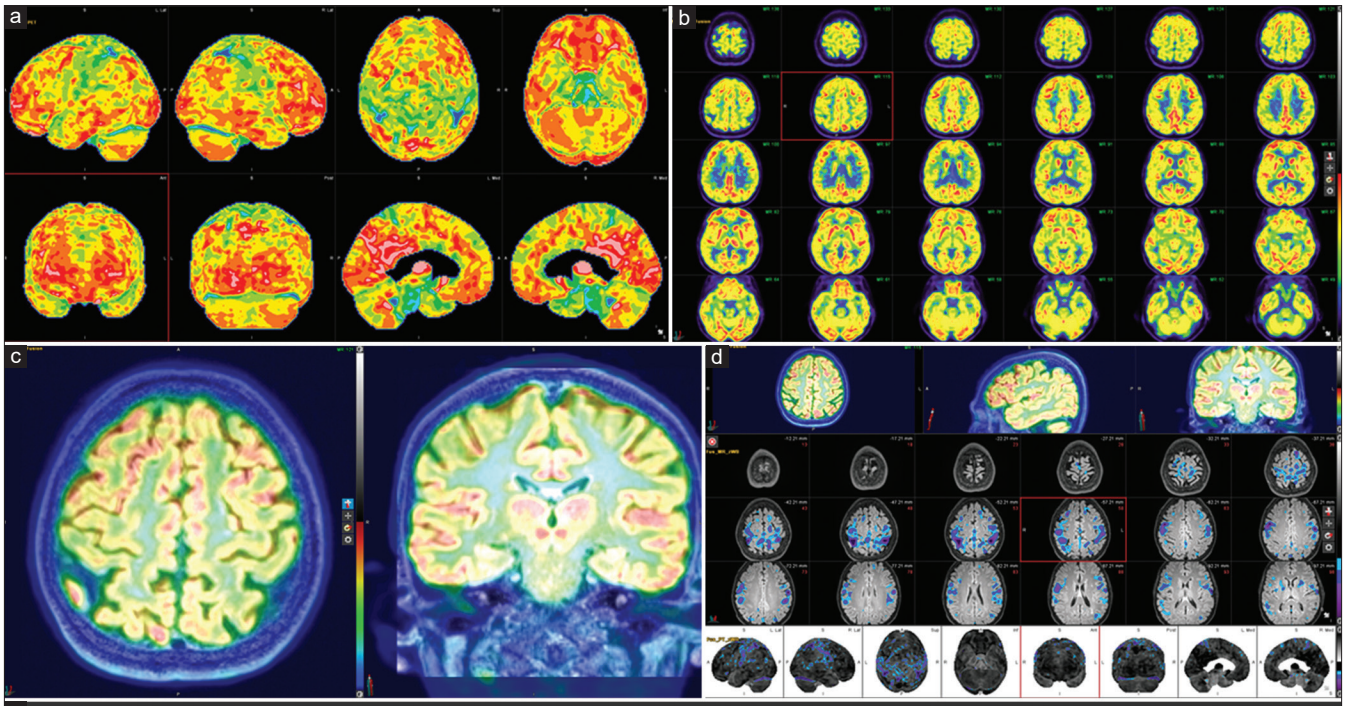

Atlas	Structure	Z-Score	L Z-Score	R Z-Score	L-R % Diff	L-R % Diff Z-Score
Single Brain Atlas	Supramarginal Gyrus	-4.34	-3.6	-2.8	0.88	-0.06
Single Brain Atlas	Parietal Lobe	-3.03	-2.47	-2.67	-0.27	-0.03
Single Brain Atlas	Angular Gyrus	-2.1	-1.65	-1.83	1.05	0.53
Single Brain Atlas	Precentral Gyrus	-2.1	-1.88	-1.69	-2.34	-0.57
Single Brain Atlas	Postcentral Gyrus	-2.04	-1.66	-1.95	0.49	0.3
Single Brain Atlas	Superior Parietal Lobule	-1.75	-1.77	-1.58	-1.37	-0.54
Single Brain Atlas	Globus Pallidus	-1.24	-0.62	-2.16	7.57	0.83

Figure 2: (a) Cortical fluorodeoxyglucose-positron emission tomography surface maps. (b) Transaxial fusion images (axial fluid-attenuated inversion recovery and positron emission tomography). (c) Select fusion fluid-attenuated inversion recovery/positron emission tomography axial image through the sensorimotor cortex and coronal views through the subcortical structures. (d) Fluid-attenuated inversion recovery-magnetic resonance imaging and positron emission tomography images with semi-quantitative Z-score overlays. (e) MIMneuro Z-Score fluorodeoxyglucose brain data in tabular format

assessment, response to pharmacotherapy, and detailed physical/neurologic exam that categorizes a primary motor or language deficit.

In patients with CBD, structural findings are often subtle and anatomic MRI sequences may reveal asymmetric atrophy involving the posterior frontal and parietal regions including atrophy of the ipsilateral primary sensorimotor cortex, corresponding to the clinically notable asymmetry in motor deficits. Furthermore, subcortical structures such as the basal ganglia, thalami, and corpus callosum may be involved, demonstrating various stages of atrophy. Corresponding FLAIR sequences may reveal white-matter hyperintensity in the atrophic frontoparietal sulci, presumably reflecting the underlying neuronal degeneration.[15,16]

In recent years, investigators have proposed functional imaging studies as an additional diagnostic imaging tool to aid in differentiating CBD from other neurodegenerative entities.[17-20] Prior ^{18}F-FDG PET brain studies demonstrated decreased regional cerebral metabolic rate most commonly in the frontal and parietal cortices of a single hemisphere as well as in the ipsilateral thalamus and basal ganglia. Furthermore, the primary sensorimotor cortex was noted to be markedly affected in some patients with CBS, which is typically spared until very late in the disease process in most other neurodegenerative syndromes. Another study revealed lower metabolism in the inferior parietal lobule, precuneus, and lateral occipital cortex of the more affected hemisphere in patients with suspected CBD. Regional asymmetries were consistently found, with more severe hypometabolism contralateral to the more involved side of the body. However, a few studies report symmetrical hypometabolism in the presence of asymmetric clinical deficits (particularly in the sensorimotor cortex) or a reversed asymmetry in a few patients.[18-20] Of note, metabolic PET

brain imaging may be particularly useful in differentiating CBD cases from other rare neurodegenerative disorders presenting with atypical parkinsonian syndromes, including PSP, due to their overlapping clinical features and oftentimes subtle findings on anatomic MRI. Specifically, patients with CBD typically demonstrate striking hemispheric asymmetry on functional imaging, with hypometabolism predominantly involving the frontoparietal cortex as well as the ipsilateral thalamus and basal ganglia, as compared to the classic anterior cortical (paramedian frontal lobe) and mesencephalic hypometabolism typically present in PSP patients.[15-16,20]

These previously described, characteristic metabolic and structural neuroimaging findings were confirmed in majority of the 12 patients in our cohort presenting with atypical parkinsonism and additional clinical features suggestive of CBD undergoing hybrid ^{18}F-FDG PET/MR imaging as part of their routine neurodegenerative disease workup, with the majority of patients demonstrating asymmetric supratentorial hypometabolism, with decreased FDG uptake particularly pronounced in the primary sensorimotor cortex (pre- and postcentral gyri), ipsilateral occipital lobe, precuneus, thalamus, and basal ganglia. However, in two of our twelve patients, we noted a more atypical pattern of striking hypometabolism centered in the precentral and postcentral gyri of the primary sensorimotor cortex bilaterally, with relative sparing of the subcortical structures and other brain regions. Furthermore, in correlating the metabolic and anatomic abnormalities of our 12 patients, the majority demonstrated congruent findings with regions of hypometabolism corresponding to structural volume loss, suggesting hypofunction of residual neurons in the regions affected by neurodegenerative process, as has been previously described in literature for other pathologies.[21]

Limitations

Limitations of this study include the retrospective nature of the research and selection of cases, predominantly dependent on our referring clinicians and as such can be skewed. In addition, there was variability in the cognitive and neuropsychological testing performed, which limited our ability to obtain a standardized neuropsychological evaluation among all patients. The small sample size and lack of pathologic confirmation of diagnosis in these cases are also inherent limitations to this work.

CONCLUSION

Advanced neuroimaging techniques, particularly hybrid brain PET/MRI studies, may help stratify patients presenting with atypical parkinsonism into more specific categories, including CBD, and allow for earlier, more specialized and targeted treatment of the underlying neurodegenerative disorder. Our study emphasizes the importance of routine assessment for two key imaging features present in patients with suspected CBD: subcortical hypometabolism ipsilateral to the cerebral hemisphere featuring decreased cortical FDG uptake and second, bilateral involvement of the pre- and postcentral gyri of the primary sensorimotor cortex.

Financial support and sponsorship

Nil.

Conflicts of interest

There are no conflicts of interest.

REFERENCES

1. He W, Goodkind D, Kowal P. U.S. Census Bureau. International Population Reports, P95/16-1, An Aging World: 2015. Washington D.C: US Government Publishing Office; 2016.
2. Gallucci M, Limbucci N, Catalucci A, Caulo M. Neurodegenerative diseases. Radiol Clin North Am 2008;46:799-817, vii.
3. Royal Society of Medicine. London, UK; 2018. Available from: http://www.nhs.uk/Corticobasal-Degeneration/treatment. [Last accessed on 2019 05]
4. Brown, RK, Bohnen NI, Wong, KK, Minoshima S, Frey KA. Brain PET in suspected dementia: Patterns of altered FDG metabolism. Radiographics 2014;34:684-701.
5. Litvan I, Grimes DA, Lang AE, Jankovic J, McKee A, Verny M, *et al*. Clinical features differentiating patients with postmortem confirmed progressive supranuclear palsy and corticobasal degeneration. J Neurol 1999;246 Suppl 2:II1-5.
6. Litvan I, Agid Y, Goetz C, Jankovic J, Wenning GK, Brandel JP, *et al*. Accuracy of the clinical diagnosis of corticobasal degeneration: A clinicopathologic study. Neurology 1997;48:119-25.
7. Boeve BF, Maraganore DM, Parisi JE, Ahlskog JE, Graff-Radford N, Caselli RJ, *et al*. Pathologic heterogeneity in clinically diagnosed corticobasal degeneration. Neurology 1999;53:795-800.
8. Tokumaru AM, O'uchi T, Kuru Y, Maki T, Murayama S, Horichi Y. Corticobasal degeneration: MR with histopathologic comparison. AJNR Am J Neuroradiol 1996;17:1849-52.
9. Armstrong MJ, Litvan I, Lang AE, Bak TH, Bhatia KP, Borroni B, *et al*. Criteria for the diagnosis of corticobasal degeneration. Neurology 2013;80:496-503.
10. Grijalvo-Perez AM, Litvan I. Corticobasal degeneration. Semin Neurol 2014;34:160-73.
11. Wang M, Gao M, Xu Z, Zheng QH. Synthesis of a PET tau tracer [(11) C] PBB3 for imaging of Alzheimer's disease. Bioorg Med Chem Lett 2015;25:4587-92.
12. Chen K, Roontiva A, Thiyyagura P, Lee W, Liu X, Ayutyanont N, *et al*. Improved power for characterizing longitudinal amyloid-β PET changes and evaluating amyloid-modifying treatments with a cerebral white matter reference region. J Nucl Med 2015;56:560-6.
13. Landau SM, Fero A, Baker SL, Koeppe R, Mintun M, Chen K, *et al*. Measurement of longitudinal β-amyloid change with 18F-florbetapir PET and standardized uptake value ratios. J Nucl Med 2015;56:567-74.
14. Shokouhi S, McKay JW, Baker SL, Kang H, Brill AB, Gwirtsman HE, *et al*. Reference tissue normalization in longitudinal 18f-florbetapir

positron emission tomography of late mild cognitive impairment. Alzheimers Res Ther 2016;8:2.
15. Boxer AL, Geschwind MD, Belfor N, Gorno-Tempini ML, Schauer GF, Miller BL, *et al*. Patterns of brain atrophy that differentiate corticobasal degeneration syndrome from progressive supranuclear palsy. Arch Neurol 2006;63:81-6.
16. Broski SM, Hunt CH, Johnson GB, Morreale RF, Lowe VF, Peller PF. Structural and Functional Imaging in Parkinsonian syndromes. Radiographics 2014;34:1273-92.
17. Seritan AL, Mendez MF, Silverman DH, Hurley RA, Taber KH. Functional imaging as a window to dementia: Corticobasal degeneration. J Neuropsychiatry Clin Neurosci 2004;16:4.
18. Whitwell JL, Jack CR Jr., Boeve BF, Parisi JE, Ahlskog JE, Drubach DA, *et al*. Imaging correlates of pathology in corticobasal syndrome. Neurology 2010;75:1879-87.
19. Lee SE, Rabinovici GD, Mayo MC, Wilson SM, Seeley WW, DeArmond SJ, *et al*. Clinicopathological correlations in corticobasal degeneration. Ann Neurol 2011;70:327-40.
20. Pardini M, Huey ED, Spina S, Kreisl WC, Morbelli S, Wassermann EM, *et al*. FDG-PET patterns associated with underlying pathology in corticobasal syndrome. Neurology 2019;92:e1121-35.
21. Samuraki M, Matsunari I, Chen WP, Yajima K, Yanase D, Fujikawa A, *et al*. Partial volume effect-corrected FDG PET and grey matter volume loss in patients with mild Alzheimer's disease. Eur J Nucl Med Mol Imaging 2007;34:1658-69.